Environmental Science & Technology

Article

Cite This: Environ. Sci. Technol. 2019, 53, 2695−2704

pubs.acs.org/est

Oxidation of Sulfonamide Antibiotics of Six-Membered Heterocyclic Moiety by Ferrate(VI): Kinetics and Mechanistic Insight into SO_2 Extrusion

Mingbao Feng,[†] J. Clayton Baum,[‡] Nasri Nesnas,[‡] Yunho Lee,[§] Ching-Hua Huang,[∥,*] and Virender K. Sharma[†,*]

[†]Department of Environmental and Occupational Health, School of Public Health, Texas A&M University, College Station, Texas 77843, United States

[‡]Department of Biomedical and Chemical Engineering and Sciences, Florida Institute of Technology, Melbourne, Florida 32901, United States

[§]School of Earth Sciences and Environmental Engineering, Gwangju Institute of Science and Technology (GIST), Gwangju 61005, Republic of Korea

[∥]School of Civil and Environmental Engineering, Georgia Institute of Technology, Atlanta, Georgia 30332, United States

Supporting Information

ABSTRACT: This work presents ferrate(VI) ($Fe^{VI}O_4^{2-}$, Fe^{VI}) oxidation of a wide range of sulfonamide antibiotics (SAs) containing five- and six-membered heterocyclic moieties (R) in their molecular structures. Kinetics measurements of the reactions between Fe^{VI} and SAs at different pH (6.5−10.0) give species-specific second-order rate constants, k_5 and k_6 of the reactions of protonated Fe^{VI} ($HFeO_4^-$) and unprotonated Fe^{VI} ($Fe^{VI}O_4^{2-}$) with protonated SAs (HX), respectively. The values of k_5 varied from $(1.2 \pm 0.1) \times 10^3$ to $(2.2 \pm 0.2) \times 10^4$ M^{-1} s^{-1}, while the range of k_6 was from $(1.1 \pm 0.1) \times 10^2$ to $(1.0 \pm 0.1) \times 10^3$ M^{-1} s^{-1} for different SAs. The transformation products of reaction between Fe^{VI} and sulfadiazine (SDZ, contains a six-membered R) include SO_2 extrusion oxidized products (OPs) and aniline hydroxylated products. Comparatively, oxidation of sulfisoxazole (SIZ, a five-membered R) by Fe^{VI} has OPs that have no SO_2 extrusion in their structures. Density functional theory calculations are performed to demonstrate SO_2 extrusion in oxidation of SDZ by Fe^{VI}. The detailed mechanisms of oxidation are proposed to describe the differences in the oxidation of six- and five-membered heterocyclic moieties (R) containing SAs (i.e., SDZ versus SIZ) by Fe^{VI}.

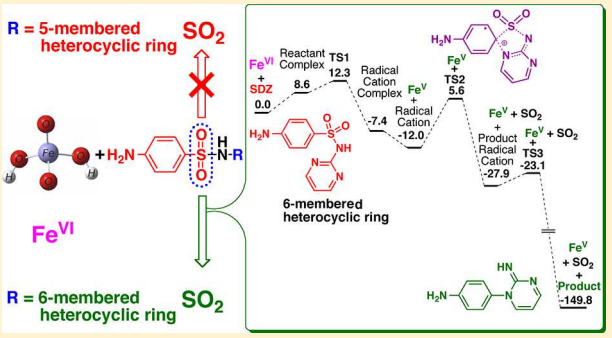

INTRODUCTION

Antibiotics have been widely used as human and veterinary medicines to treat infections and to enhance animal growth.[1−3] The consumption of antibiotics has increased because of an increase in the world population and the aging population in industrialized countries.[4,5] Significant portions of the antibiotics are excreted in feces and urine without metabolization. An overuse of antibiotics has caused growing concern because their release from hospitals, wastewater treatment plants, and livestock farms into the environment presents potential risks to human health and ecosystems. Among the antibiotics, sulfonamides (SAs) have been extensively used, which may result in ecological health hazards, food contamination, and pollution of drinking water supplies as well as the development of antibiotic resistant bacteria (ARBs) and antibiotic resistant genes (ARGs).[6−8]

Many investigations have been carried out to treat SAs in water before their release into the environment, such as biological treatment, adsorption, membrane processes, chlorination, electrochemical means, and advanced oxidation technologies.[9−18] This current work pertains to the use of the chemical oxidant, ferrate(VI) ($Fe^{VI}O_4^{2-}$, Fe^{VI}), on which several studies on its application to treat micropollutants have appeared in the past decade.[19−23] Few investigations, including some studies from our laboratory, have been carried out on the kinetics and mechanisms of the oxidation of SAs by Fe^{VI}.[24−28] SAs contain two aromatic moieties: an aniline ring and a heterocyclic N-containing aromatic ring (R) that are joined through a sulfonamide linkage (−NH−SO_2−) (Figure 1). The R can be either a five- or a six-membered ring. Most of the studies on the oxidation of SAs by Fe^{VI} were performed on

Received: November 19, 2018
Revised: January 27, 2019
Accepted: February 4, 2019
Published: February 4, 2019

DOI: 10.1021/acs.est.8b06535
Environ. Sci. Technol. 2019, 53, 2695−2704

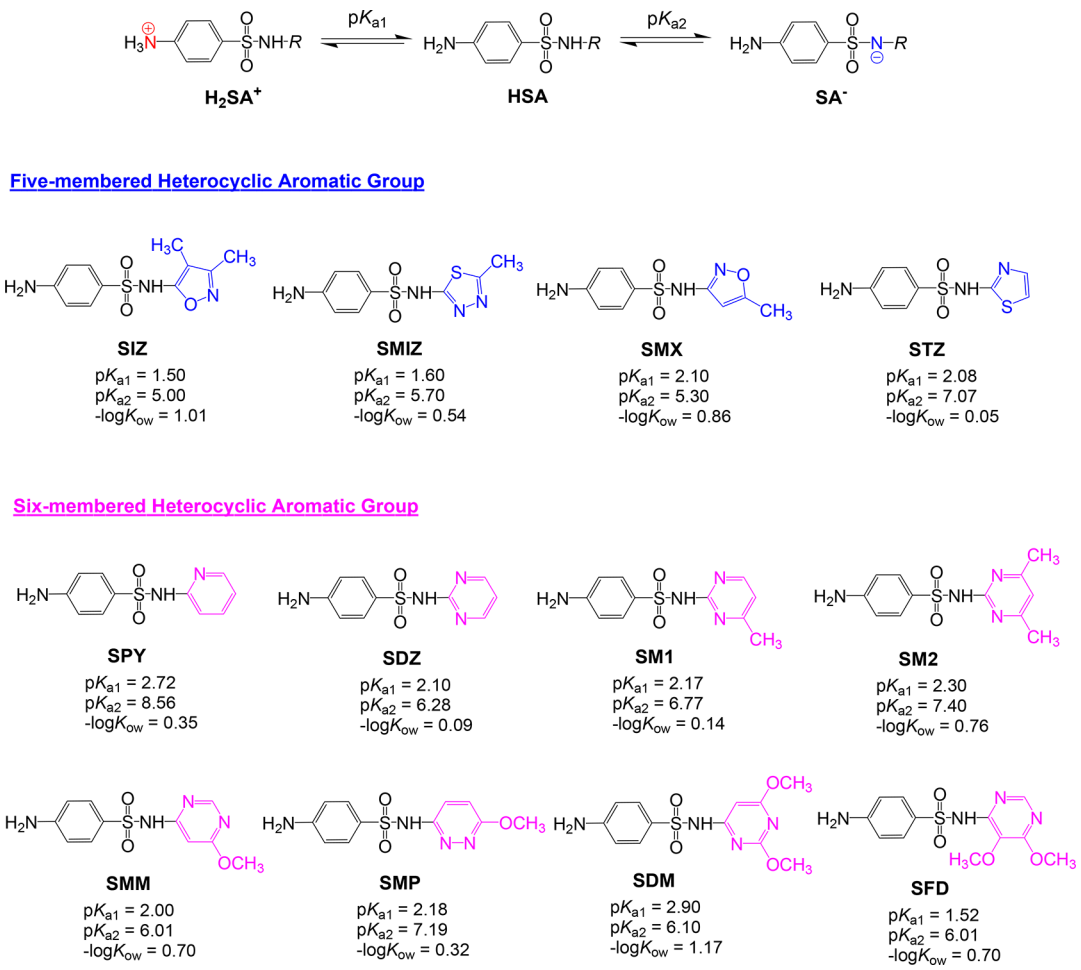

Figure 1. Molecular structures of sulfonamide antibiotics (SAs) and their dissociation constants and logK_{ow} values.

sulfamethoxazole (SMX) containing a five-membered *R*. Products seen were from the attacks by Fe^{VI} on the aniline and the moieties of *R*.[24,25,27,28] The research in the present work is stimulated from our recent product analysis on the oxidation of sulfadimethoxine (SDM) by Fe^{VI} that showed extrusion (or release) of SO_2 during the transformation of the parent molecule.[29] SDM contains a six-membered *R*. Comparatively, products identified in the oxidation of SMX by Fe^{VI} showed no extrusion of SO_2 from the parent molecule.[24,25,27,28] We thus question if the extrusion of SO_2 is related to the heterocyclic ring (i.e., five- or six-membered *R*) of the SAs. To further clarify the mechanisms, we selected sulfadiazine (SDZ) and sulfisoxazole (SIZ), individually containing six- and five-membered *R* in their structures, respectively, and monitored their transformation products in reactions with Fe^{VI}. We hereby demonstrate for the first time that the extrusion of SO_2 by metal-based oxidant depends on the heterocyclic moiety of the SAs (i.e., *R*).

The formation of SO_2 extrusion products has been reported during the transformation of SAs with a six-membered *R* by photodegradation,[30] sulfate radical-based oxidation,[9,31,32] horseradish peroxidase,[10] chlorination,[33] and permanganate.[34] In these studies, reaction pathways have been given without any mechanistic details on how the oxidant is involved in the reaction steps. This information is available on describing photochemical oxidation of aqueous SAs using theoretical approaches.[35] In the current paper, we performed density functional theory (DFT) calculations to elucidate the SO_2 extrusion step of the mechanism via single electron transfer (SET) as an initial step. The obtained transition states (TS) of DFT calculation clearly show the ability of SO_2 extrusion from SAs containing a six-membered *R*. This is the first example of Fe^{VI} inducing SO_2 extrusion, via a single electron transfer initiation step. We also provide an explanation for the absence of SO_2 extrusion in SAs that bear a five-membered ring in the presence of Fe^{VI}. The role of the heterocyclic ring substituent (*R*) of SAs was further elaborated via kinetics studies of the reaction between Fe^{VI} and SAs with varying *R* substituents (Figure 1) as a function of pH (6.5−10.0).

The overall aims of the paper are to (i) determine species-specific rate constants (k) of the reactions between Fe^{VI} and SAs, (ii) identify the transformation products of the oxidation of SDZ and SIZ by Fe^{VI} using a high-resolution liquid chromatography−mass spectrometry (HR-LC−MS) technique, (iii) apply quantum chemical calculations and transition state theory to elucidate the SO_2 extrusion mechanism of SDZ by Fe^{VI}, and (iv) compare the oxidation of SAs with five-membered and six-membered *R* to learn when the formation of SO_2 extrusion products from the SAs is feasible.

MATERIALS AND METHODS

Chemicals and Reagents. Detailed information on the test SAs (sulfisoxazole (SIZ), sulfamethizole (SMIZ), sulfamethoxazole (SMX), sulfathiazole (STZ), sulfapyridine

DOI: 10.1021/acs.est.8b06535
Environ. Sci. Technol. 2019, 53, 2695−2704

Table 1. Species-Specific Rate Constants for Oxidation of SAs by Fe^{VI} at 25.0 °C

SAs		pK_{a2}	k_s (M^{-1} s^{-1})	k_6 (M^{-1} s^{-1})	R^2	source
five-membered heterocyclic aromatic group	SIZ	5.00[28]	$(1.1 \pm 0.1) \times 10^4$			28
	SMIZ	5.70[28]	$(2.2 \pm 0.2) \times 10^4$			28
	SMX	5.30[28]	$(7.0 \pm 0.5) \times 10^3$			28
	STZ	7.07[45]	$(1.2 \pm 0.1) \times 10^3$	$(1.1 \pm 0.1) \times 10^2$	0.938	this study
six-membered heterocyclic aromatic group	SPY	8.56[46]	$(2.7 \pm 0.3) \times 10^3$	$(2.1 \pm 0.1) \times 10^2$	0.971	this study
	SDZ	6.28[45]	$(1.5 \pm 0.1) \times 10^3$	$(9.0 \pm 0.1) \times 10^2$	0.979	this study
	SM1	6.77[45]	$(1.6 \pm 0.1) \times 10^3$	$(9.0 \pm 1.0) \times 10^2$	0.999	this study
	SM2	7.40[28]	$(1.9 \pm 0.1) \times 10^3$	$(2.25 \pm 0.2) \times 10^2$		28
	SMM	6.01[45]	$(4.5 \pm 0.2) \times 10^3$	$(6.0 \pm 0.5) \times 10^2$	0.997	this study
	SMP	7.19[47]	$(1.8 \pm 0.2) \times 10^3$	$(1.0 \pm 0.1) \times 10^3$	0.954	this study
	SDM	6.10[28]	$(1.88 \pm 0.04) \times 10^4$			24
	SFD	6.01[48]	$(5.2 \pm 0.2) \times 10^3$	$(6.5 \pm 0.4) \times 10^2$	0.964	this study

(SPY), sulfadiazine (SDZ), sulfamerazine (SM1), sulfamethazine (SM2), sulfamonomethoxine (SMM), sulfamethoxypyridazine (SMP), sulfadimethoxine (SDM), and sulfadoxine (SFD)), Fe^{VI}, buffers, and preparation of all reaction solutions is provided in Text S1 of the Supporting Information (SI).

Stopped-Flow Experiments. Experiments were carried out under pseudo-first-order conditions to perform the kinetics of the reactions between Fe^{VI} and seven different kinds of SAs (i.e., STZ, SPY, SDZ, SM1, SMM, SMP, and SFD). Under these conditions, the concentrations of SAs ($5.0-10.0 \times 10^{-4}$ M) were higher than Fe^{VI} (5.0×10^{-5} M). The kinetic measurement was performed using a stopped-flow spectrophotometer (SX-20 MV, Applied Photophysics, Surrey, U.K.). Details are provided in Text S2 and Figure S1.

Oxidized Products Experiments. The identification of the oxidized products (OPs) of SDZ (4.0×10^{-5} M) or SIZ (4.0×10^{-5} μM) by Fe^{VI} (2.0×10^{-4} M) at pH 9.0 was conducted by the solid phase extraction-liquid chromatography-high-resolution/accurate mass (HR/AM) spectrometry (SPE-LC–HRMS) technique (Text S2).[36] The analysis of OPs by the other oxidants aided us to identify the transformation of SDZ by Fe^{VI}.[31,32]

Quantum Chemical Calculations. All calculations were performed with the Gaussian 09 program[37] using primarily the unrestricted M06 DFT functional[38] with the 6-311++G(d,p) basis set. Details are provided in Text S3.

The structure of each species with bond lengths is provided in Figure S2 along with a table of enthalpies and Gibbs free energies (Table S1). The charges and spin densities for all species were calculated with Hirshfeld population analysis[39–41] and are given in Table S2 and Figures S3 and S4, respectively. Additionally, the atomic labeling of SDZ is provided in Figure S5. The zero-point-energy-corrected Gibbs free energy scale was chosen since the Gibbs free energy of activation can be related directly to the experimental rate constants.[42]

Eighteen kinds of representative quantum chemical descriptors of all 12 SAs after structural optimization were calculated using the unrestricted M06 DFT functional with the 6-311++G(d,p) basis set to investigate their possible correlations with the observed species-specific rate constants by Fe^{VI}. These parameters included the energy of the highest occupied molecular orbitals (E_{HOMO-n}, $n = 0-5$), the energy of the lowest unoccupied molecular orbital (E_{LUMO}), the energy difference of E_{HOMO} and E_{LUMO} (ΔE ($E_L - E_H$)), the most negative net charge in the atom of the molecule (q^-), the most positive net atomic charge on a H atom (qH^+), dipole moment (μ), average polarizability (α), ionization potential (IP), electron affinity (EA), hardness (η), softness (S), electronegativity (ζ), and electrophilicity index (ω). The obtained values with the SMD solvent model are presented in Table S3. The correlation analysis was conducted using SPSS software (Version 16.0).

RESULTS AND DISCUSSION

Kinetics. In this study, additional SAs were included to learn the trend of variation of rates with SAs containing R of five- and six-membered moieties. An approach used to determine the second-order rate constant (k, M^{-1} s^{-1}) of the reaction between Fe^{VI} and SAs was similar to earlier kinetic investigations (eq 1).[24,25,28]

$$-d[Fe^{VI}]/dt = k[Fe^{VI}][SA] \quad (1)$$

The values of k at different pH were determined from 6.5 to 10.0. Results are presented in Figure S6. Rates were decreased with an increase in pH, and the pattern was similar in the reactions of Fe^{VI} with several inorganic and organic compounds.[23,43]

The variation in the values of k with pH was interpreted quantitatively using acid–base equilibrium of Fe^{VI} and SAs. In the pH range of the study, only monoprotonated and unprotonated species of Fe^{VI} and SAs (X) are involved (eqs 2 and 3).[28,44–48]

$$HFeO_4^- \rightleftharpoons H^+ + FeO_4^{2-}, \quad pK_{a3} = 7.23 \quad (2)$$

$$HX \rightleftharpoons H^+ + X^-, \quad pK_{a2} = 5.00 - 8.56 \quad (3)$$

The dependence of k on the pH can thus be modeled by eq 4.

$$-d[X]/dt = k[Fe^{VI}]_{tot}[X]_{tot} = \Sigma k_{ij}\alpha_i\beta_j[Fe^{VI}]_{tot}[X]_{tot} \quad i = 1, 2 \quad j = 1, 2 \quad (4)$$

where $[Fe^{VI}]_{tot} = [HFeO_4^-] + [FeO_4^{2-}]$; $[X]_{tot} = [HX] + [X^-]$; α_i and β_j represent the species fractions of Fe^{VI} and selected SA, respectively; i and j are each of the species of Fe^{VI} and selected SA, respectively; and k_{ij} is the species-specific second-order rate constant for the reaction between the Fe^{VI} species i and the X species j. Overall, four reactions could possibly contribute to eq 4.

Equation 4 was applied to empirically fit the kinetic data of the oxidation of SAs by Fe^{VI} in Figure S6. It was observed that only two of the four reactions were needed to reasonably fit the

DOI: 10.1021/acs.est.8b06535
Environ. Sci. Technol. 2019, 53, 2695–2704

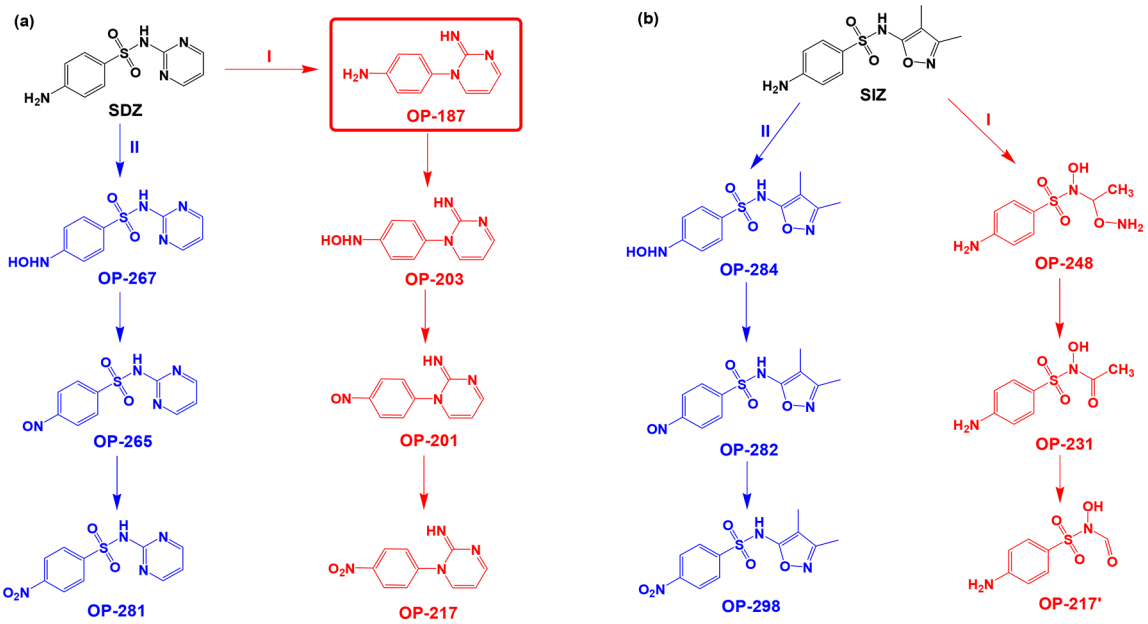

Figure 2. Proposed transformation pathways of SDZ (a) and SIZ (b) by Fe^{VI} (experimental conditions: [SDZ] = [SIZ] = 4.0×10^{-5} M, [Fe^{VI}] = 2.0×10^{-4} M, pH = 9.0, T = 25.0 °C).

experimental data (see solid lines in Figure S6). These two reactions are presented by eqs 5 and 6.

$$HFeO_4^- + HX \rightarrow \text{products} \quad (5)$$

$$FeO_4^{2-} + HX \rightarrow \text{products} \quad (6)$$

Values of the species-specific rate constants, k_5 and k_6, for the reactions 5 and 6, respectively, are given in Table 1. Values of k_5 were found in the range from $(1.2 \pm 0.1) \times 10^3 - (2.2 \pm 0.2) \times 10^4$ M^{-1} s^{-1}, while the range of k_6 was from $(1.1 \pm 0.1) \times 10^2$ to $(1.0 \pm 0.1) \times 10^3$ M^{-1} s^{-1}. It seems that the variation in k_5 is related to change in R, which influences the aniline moiety, the attacking site by Fe^{VI} in oxidizing SAs. More is discussed in later sections. The reaction between Fe^{VI} and SAs has proton ambiguity, i.e., the reaction of $HFeO_4^-$ with X^- is involved instead of reaction 6 (i.e., FeO_4^{2-} + HX). The reactivity of protonated Fe^{VI} (or $HFeO_4^-$) with X^- would be faster than that with HX due to higher electron density on the X^-. This possibility may occur because FeO_4^{2-} is a weaker oxidant than $HFeO_4^-$. However, the kinetics measurements of our study do not fully distinguish which of the two reactions would be preferable.

In the case of sulfadiazine (SDZ), the kinetics of the reaction with Fe^{VI} were extended to the acidic pH range (Figure S6). This allowed the calculation of the rate constant values of the reaction between diprotonated Fe^{VI} and protonated SDZ (or HX) as $(2.7 \pm 0.5) \times 10^4$ M^{-1} s^{-1}. The result suggests that the reactions of Fe^{VI} with the protonated species of SDZ follow the order of reactivity as H_2FeO_4 > $HFeO_4^-$ > FeO_4^{2-}. Overall, results of different SAs showed that the protonated Fe^{VI} ($HFeO_4^-$) reacted faster with SAs than the unprotonated Fe^{VI} (FeO_4^{2-}) (i.e., $k_5 > k_6$). It has been suggested that the partial radical character of Fe^{VI} ($Fe^{VI} = O \leftrightarrow Fe^{V} - O^{\bullet}$) is proton stabilized to yield higher reactivity of protonated species than the unprotonated species of Fe^{VI}.[49] Furthermore, the oxo ligands in $HFeO_4^-$ have larger spin density than in FeO_4^{2-} that result in increased oxidation ability of protonated Fe^{VI}.[50,51] The fraction of the $HFeO_4^-$ (α_{HFeO4-}) decreased with increase in pH, and hence the overall rate constant of the reactions between Fe^{VI} decreased with increase in pH (see Figure S6).

Understanding of the variation of rates for the oxidation of SAs by Fe^{VI} was attempted by calculating molecular structure descriptors of SAs. A total of 18 kinds of these descriptors were obtained using the unrestricted M06 DFT functional with the 6-311++G(d,p) basis set, which included E_{HOMO-n} (n = 0–5), E_{LUMO}, ΔE ($E_L - E_H$), q^-, qH^+, μ, α, IP, EA, η, S, ζ, and ω (Table S3). A similar approach has been applied in understanding the reactivity of organic pollutants with Fe^{VI}[52] and other oxidants.[52−56] The rate constants showed no significant correlation with any individual descriptor (Table S4); therefore, no further evaluation of variation of rate constants of different SAs using the calculated molecular descriptors was performed.

Oxidized Products and Reaction Pathways. In this study, the oxidized products (OPs), generated via the oxidation of SDZ (a representative SA with six-membered heterocyclic group) and SIZ (a representative SA with five-membered heterocyclic group) by Fe^{VI}, were characterized using high-resolution LC−MS (ESI pos). Structural assignments of OPs were performed by product ion scans, based on the corresponding MS/MS spectra and their proposed fragmentation patterns. The detailed data and proposed structures of the OPs and their MS/MS fragments are shown in Table S5 and Figures S7 and S8. Errors of m/z between the experimental and theoretical values errors were mostly <3 ppm. It is necessary to analyze the mass spectrum of the parent compound and the fragment losses generated, which may also be detected in the structural identification of the OPs.[57,58] For example, SDZ (m/z 251.06027 and R_t at 2.62 min) has four main product ions at 156.01183 and 96.05644, 108.04513, and 92.05033, corresponding to the cleavage of the S−N bond in SDZ, and losses of SO (48 Da from 156.01183) and SO_2 (64 Da from 156.01183), respectively (Figure S7a). Although some MS/MS information regarding the OPs of SDZ and SIZ by Fe^{VI} oxidation is lacking, recent investigations of trans-

DOI: 10.1021/acs.est.8b06535
Environ. Sci. Technol. 2019, 53, 2695−2704

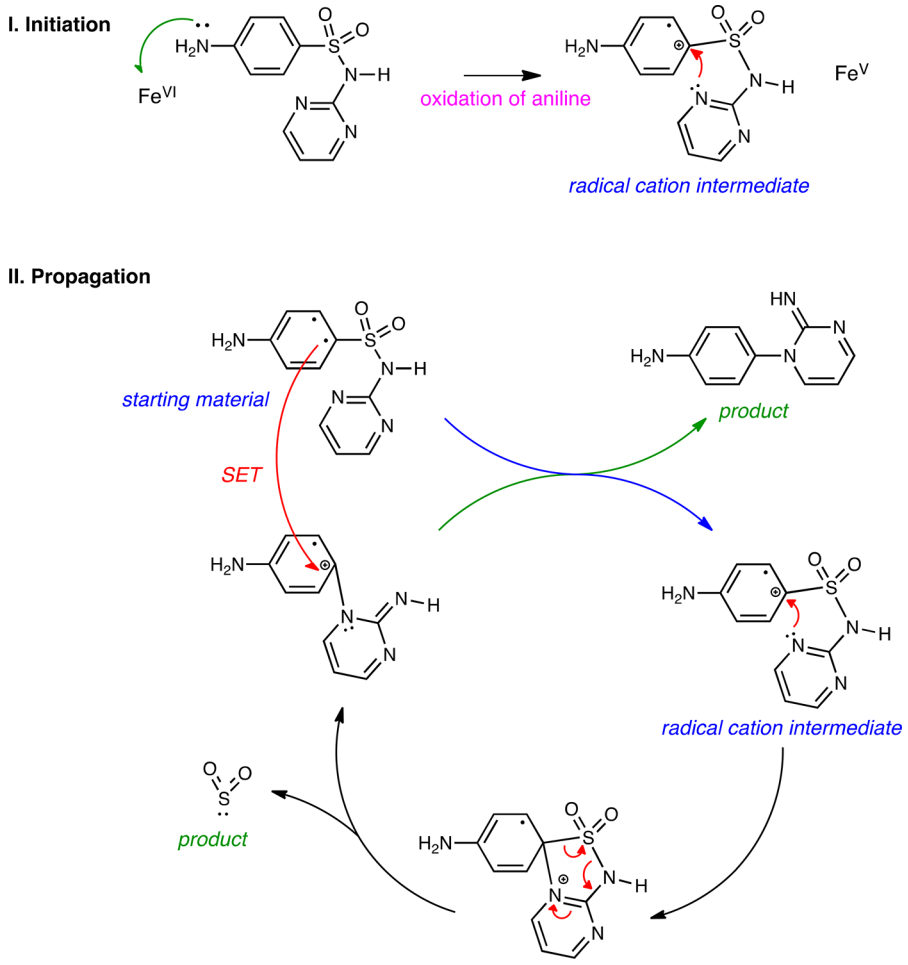

Figure 3. Plausible mechanism of Fe^{VI}-catalyzed extrusion of SO_2 from SDZ and other aminopyridine-type sulfa drugs, via initiation of an oxidative single electron transfer from the aniline moiety.

formation products of these two SAs could facilitate the structural identification of these OPs.[9,10,31−34]

Representatively, OP-187 with a protonated form at *m/z* 187.09831 and chromatographic retention time at 5.22 min was proposed in our study as the product generated from the SO_2 extrusion in SDZ molecule (Table S5 and Figure S7e). This structure was confirmed by six detected product ions at *m/z* 170.07178, 160.08734, 108.06863, 92.05029, and 65.03954. These MS/MS fragments corresponded to the individual losses of such fragments as NH_3 (17 Da from 187.09831), CN (27 Da from 187.09831), C_3H_2N (52 Da from 160.08734), NH_2 (16 Da from 108.06863), and CN (27 Da from 92.05029), respectively. Similarly, in view of the repeated MS/MS fragments and proposed fragmentation patterns of the OPs of SDZ and SIZ, the individual structures of OP-281, OP-217, OP-201, OP-187, OP-298, OP-282, OP-248, OP-231, and OP-217' were proposed, and the possible fragmentation pathways are shown in Figures S7 and S8. It is difficult to obtain the MS/MS spectra of the OPs with low MS intensity (i.e., OP-267, OP-265, OP-203, and OP-284). Therefore, the structures of such OPs were thus tentatively proposed based on the accurately measured molecular compositions (Table S5) and the possible transformation pathways.

On the basis of the structures of the identified OPs, the proposed transformation pathways of SDZ and SIZ by Fe^{VI} at pH 9.0 are presented in Figure 2. An initial oxidative attack on the aniline site of SDZ by Fe^{VI} is suggested, which can lead to the two products: the SO_2 extrusion and the hydroxylation of the aniline ring. In pathway I, Fe^{VI} can initiate a single electron transfer oxidative pathway of the aniline ring, resulting in a radical cation and Fe^{V}. The cation in turn induces the SO_2 extrusion of SDZ leading to OP-187 (Figure 2a). Fe^{V} has a much higher reactivity than Fe^{VI} and may participate in the oxidation of SDZ alongside Fe^{VI}.[59,60] The intermediates resulting from a potential Fe^{V} oxidation would be identical to those resulting from the single electron transfer observed with Fe^{VI}. However, the self-decomposition of Fe^{V} is fast with a rate constant of order of 10^7 M^{-1} s^{-1}.[49] The competing rate constants of the reaction of Fe^{V} with SDZ and its self-decomposition would determine the involvement of Fe^{V} in the reaction mechanism.

It should be noted that OP-187 is itself not any more oxidized than SDZ, rather, formed as a result an unprecedented catalytic effect of Fe^{VI}. However, subsequent oxidation of OP-187 proceeded by hydroxylation of the aniline ring to form OP-203 with an −NHOH group, which was successively oxidized to generate OP-201 with an −NO group and OP-217 with an -NO_2 group (Figure 2a). Pathway II was initiated by hydroxylation in the aniline ring of SDZ, with the resultant product of OP-267. Afterward, similar reaction steps like pathway I after SO_2 extrusion occurred to yield OP-265 and OP-281 (Figure 2a).

DOI: 10.1021/acs.est.8b06535
Environ. Sci. Technol. 2019, 53, 2695−2704

In the oxidation of SIZ by Fe^{VI}, pathway I involved ring opening of the five-membered isoxazole ring and hydroxylation taking place on the N atom between the two rings of SIZ (Figure 2b), resulting in the formation of OP-248. Opening of the isoxazole ring has also been suggested during Fe^{VI} oxidation of SMX.[24,28] This ring opening may involve the $-NH-SO_2-$ group in SMX because isoxazole itself has no reactivity with Fe^{VI}. Theoretical investigations suggested that this step was initiated via nucleophilic attack of Fe^{VI} followed by isomerization, H-bond assisted C−O cleavage and Fe−O bond cleavage.[27] With the reaction progressing, further attacks on the heterocyclic ring happened to generate OP-231 and OP-217′. Similar to pathway II of SDZ, OP-284, OP-282, and OP-298 were produced in pathway II of SIZ (Figure 2b). Overall, these identified OPs allowed the enhanced understanding of oxidation of SAs by Fe^{VI}.

Possible reaction mechanisms of hydroxylation of SDZ (Figure S5) to form OP-267 in pathway II can, in principle, occur on either the aniline N or the sulfonamide N, leading to products of identical masses. In basic pH, the sulfonamide N may become deprotonated and will therefore be more susceptible to oxidation. Hydroxylation of either N atoms can be achieved via two plausible pathways: (i). Sequential two single-electron transfer to Fe^{VI} leading to Fe^{IV}, and subsequent trapping by water and loss of a proton as described in our earlier work on SMX,[24] or (ii). A direct oxygen transfer from Fe^{VI} to the N of aniline in SAs, followed by rapid proton transfer from the resulting ammonium salt to the N-oxide leading to hydroxylamine (Figure S9).

Fe^{VI} Oxidation of SDZ—SO_2 Extrusion. Two pathways are proposed in which Fe^{VI} oxidizes either of the two aromatic rings of SDZ via a single-electron transfer leading to Fe^{V} (Figures 3 and S10). Figure 3 corresponds to single-electron transfer from aniline ring. The electron-transfer from *R* (pyrimidine ring) of SDZ is another possibility (Figure S10). These mechanistic pathways are unique to SAs containing a six-membered ring with a nitrogen ortho to the amido nitrogen. The presence of the ortho nitrogen heteroatom enables the formation of a five-membered ring intermediate initiated by any number of pathways including oxidative conditions ($SO_4^{\bullet-}$ and Fe^{VI}) or photochemical excitation to triplet states.[30,32] The formation of a five-membered ring annihilates the aromaticity of the aniline ring, therefore raising the energy by close to 18 kcal/mol according to our computations. The extrusion of SO_2 then becomes plausible to restore aromaticity (Figure 3), or to generate another intermediate that will itself act as an oxidant to another molecule of the SA leading to a radical cation intermediate and subsequently restoring the aromaticity which leads to the SO_2 extruded product. Although these reactions are occurring in the presence of the strong oxidant Fe^{VI}, the overall extrusion of SO_2 and rearrangement is not a net oxidative pathway, and Fe^{VI} is acting to initiate the catalytic cycle (i.e., chain reactions). This is supported by the observed products discussed in the prior section.

Transition State Calculations. The calculations for the radical cation intermediate support oxidation according to Figure 3 rather than Figure S10. In other words, *R* is not involved in initial oxidation of SDZ by Fe^{VI} (i.e., ruling out the possibility of single-electron transfer as depicted in Figure S10). As stated earlier in the experimental method, C1−C6 are carbon atoms and N17 is N atom of the aniline ring (see Figure S5 for labels). The spin density is almost entirely on the aniline ring (see Figures S4), indicating that the unpaired electron in the radical resides on that ring. The two largest values are on C5 (0.26) and N17 (0.29). Likewise, the largest positive increase in charge in oxidizing SDZ occurs on the aniline ring, especially the amino N17 (0.1705) (see Table S2). These results suggest that C5 and N17 are likely to be active participants in succeeding steps. Additionally, the diprotonated Fe^{VI} was chosen for transition state calculations since it reacts most readily with SDZ. The optimized structural parameters of all chemical species involved are briefly discussed below.

$H_2Fe^{VI}O_4$ vs $H_2Fe^{V}O_4^-$. $H_2Fe^{VI}O_4$ has shorter computed bond lengths, Fe−OH 1.76 Å vs 1.86 Å and Fe = O 1.59 (1.56) Å vs 1.62 Å than $H_2Fe^{V}O_4^-$, as a result of less electron repulsion. The charge on Fe is more positive, +0.55 vs +0.42, and the oxygen atoms are less negative, −0.25 vs −0.42, because there is one less electron. Also, the spin density is lower, 1.68 vs 2.63, on Fe^{VI} because there is one less unpaired electron.

SDZ vs SDZ Radical Cation. The atomic charges on the radical cation are best interpreted by comparison with SDZ (Table S2). The column to the right gives the difference in charge between the cation and SDZ. Notice that there is a much more positive increase on the aniline ring with the largest increase on N17 even though the N17 charge in the cation is only slightly positive (see Figure S5 for the atom numbering). The unpaired electron resides largely on N17 and C5, as indicated by the spin density. The changes in bond lengths are more subtle, with the H17−C2 bond becoming 0.04 Å shorter and the C5−S7 bond stretching by 0.04 Å.

Reactant Complex. An H-bonded complex is formed between the $H_2Fe^{VI}O_4$ and SDZ. The H-bond involves an O−H group on the Fe^{VI} with N17 on SDZ. The primary contribution of the H-bond is to bring the two molecules close enough together that transfer of an electron can occur. The N17−C2 bond and O−H Fe^{VI} bond both increase by 0.03 Å as a result of the H-bond. The charge on N17 is slightly less negative. However, the zero spin densities on SDZ indicate that no electron has been transferred.

TS1. The H-bond involving N17 on SDZ and an O−H group on the Fe^{VI} has broken and a new H-bond is forming, involving N17−H26 on SDZ and an O on the Fe^{VI}. As a result, the charge on N17 has become 0.06 more negative. The spin density indicates no electron transfer at this stage. The principal action is the change in H-bonding.

Radical Cation Complex. The new H-bond has formed between N17−H26 on SDZ and an O on the Fe^{VI}. At the same time, an electron has transferred from SDZ to the Fe^{VI} as indicated by the nonzero spin densities on SDZ, principally 0.32 on N17, 0.25 on C5, 0.19 on C1, and 0.17 on C3 that result from the loss of an electron. Likewise, the spin density on Fe has increased from 1.70 to 2.67 as a result of an additional unpaired electron. After oxidation occurs, there are now three unpaired electrons on the Fe^{VI} and one unpaired electron on SDZ. With a total of four unpaired electrons, one might consider the spin state for the complex to be a quintet. However, much better results were obtained for the triplet spin state, indicating that the unpaired electron on SDZ remains opposite in spin to the added electron on Fe^{VI}. This in turn indicates that the complex is so loose that Hund's rule does not apply. Consistent with the electron transfer, the Fe^{VI} has become less positive and the oxygen atoms more negative, and SDZ is overall more positive with the principal changes on N17.

DOI: 10.1021/acs.est.8b06535
Environ. Sci. Technol. 2019, 53, 2695−2704

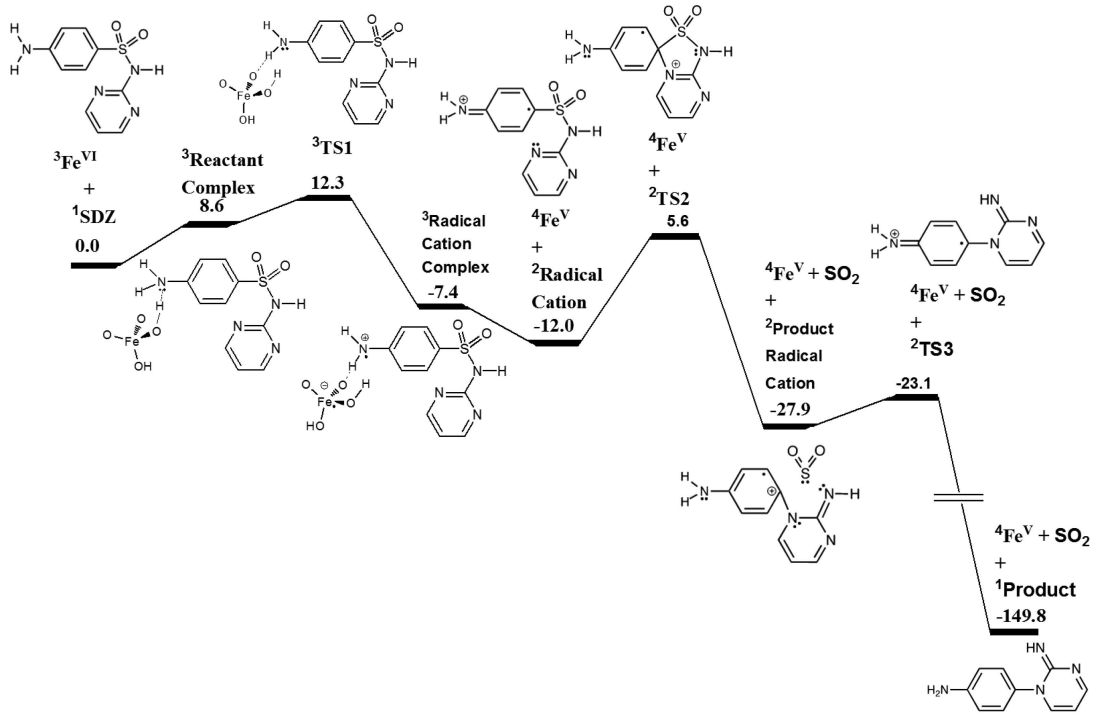

Figure 4. Free energy pathway (kcal/mol) of SO_2 extrusion and rearrangement of SDZ in the presence of diprotonated Fe^{VI} to produce OP-187. Only the organic structures are drawn.

As a consequence of the electron transfer, all the Fe−O bonds have increased. The N17−C2 bond has decreased to 1.32 Å. The aniline ring has become more quinoidal and the C5−S7 bond has increased to 1.79 Å.

SDZ Radical Cation. There is very little geometry change as the complex dissociates to form the radical cation and $H_2Fe^VO_4^-$. There also is no significant change in either the charges or the spin densities. Since the complex has dissociated, the spin states for Fe^{VI} and the SDZ radical cation are now quartet and doublet, respectively.

TS2. An intrinsic reaction coordinate calculation (IRC) involving TS2 is very illuminating. As TS2 is approached, the C5−N12 distance decreases while the C5−S7 bond is stretched. The C5−C7 bond is broken shortly after the top of the energy barrier, and after that the C5−N12 bond is formed. Finally, the S7−C10 bond is broken, releasing SO_2. The TS2 structure can be considered to include a five-membered ring although some bond lengths are stretched, especially the C5−N12 distance (1.79 Å vs 1.40 Å in the product radical cation) but also N10−S7 (1.74 Å vs 1.66 Å in SDZ radical cation) and S7−C5 (1.89 Å vs 1.79 in SDZ radical cation).

Product Radical Cation. As before, the unpaired electron is almost entirely on the aniline ring, principally N17 and C5. Likewise, the positive charge is located principally on the aniline ring. The most negative charge (−0.29) is on N10, now exo to the diazine ring.

TS3. Only the doublet state is stable, which means that there is still one unpaired electron. Thus, the bond lengths, charges, and spin densities are all very similar to the product radical cation. The major change occurring as TS3 is approached is that the two ring systems are becoming more planar; the dihedral angle between the two planes increases from 136° in the product radical cation to 178° in TS3.

Product. The aniline ring returns from a quinoidal structure to an aromatic structure with nearly equal C−C bond lengths. The C2−N17 and C5−N12 bond lengths have both increased, and the dihedral angle between the two rings has decreased significantly to 111° to minimize steric interaction. The charges on the aniline ring are similar to those in SDZ. Like the product radical cation, the most negative charge (−0.37) is on N10.

The Gibbs free energy pathway for diprotonated Fe^{VI} and SDZ is shown in Figure 4. The diprotonated Fe^{VI} and SDZ form an H-bonded reactant complex involving a hydroxyl H on the Fe^{VI} and the negatively charged N17 on SDZ. Although this H-bond lowers the enthalpy by 4.8 kcal/mol, the entropy loss increases the free energy by 8.2 kcal/mol. The transition state (TS1) involves breaking of the original H-bond and formation of a new H-bond between an amino H on SDZ and an O on Fe^{VI} along with transfer of an electron from SDZ to Fe^{VI}, forming a radical cation complex with Fe^V. This complex dissociates to give the more stable radical cation and Fe^V as separate species. Thus, the sole role of Fe^{VI} is the oxidation of SDZ. The expected large energy required to oxidize SDZ is offset by the difference between Fe^V and Fe^{VI}, $\Delta H = -143.1$ and $\Delta G = -144.4$ kcal/mol (Table S1).

The SDZ radical cation goes through another transition state (TS2) to form the product radical cation, releasing SO_2. It is interesting that while molecular mechanics (UFF) and semiempirical (PM6) calculations predict a stable five-membered ring intermediate as shown in Figure 3, DFT calculations do not. However, TS2 is close to the formation of the five-membered ring. As an azine nitrogen (N12) is forming a bond with C5 to form the five-membered ring, the C5−S7 bond starts to break, followed by dissociation of the N10−S7 bond to release SO_2. Formation of the much more stable final, neutral product is very exothermic with a low barrier (TS3).

DOI: 10.1021/acs.est.8b06535
Environ. Sci. Technol. 2019, 53, 2695−2704

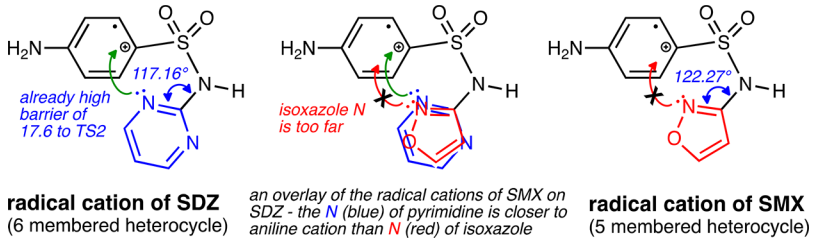

Figure 5. Difference in geometries between the five-membered ring of isoxazole in SMX and the six-membered ring of pyrimidine in SDZ. Comparison of their radical cations clarifies the reasoning behind why only SDZ undergoes SO_2 extrusion.

The net oxidation of SDZ to give the product plus SO_2 has a ΔH = +7.1 kcal/mol and ΔG = −5.3 kcal/mol (Table S1).

The oxidation step is rate determining as indicated by TS1 having the highest energy (12.3 kcal/mol) relative to the reactants. This corresponds to a rate constant of 5.7×10^3 M^{-1} s^{-1} for H_2FeO_4 in good agreement with the experimental value of 2.7×10^4 M^{-1} s^{-1}. Further confirmation of this mechanism is that the TS1 barrier height for $HFeO_4^-$ oxidation of SDZ is calculated to be 13.9 kcal/mol, corresponding to a rate constant of 4.0×10^2 M^{-1} s^{-1} compared to the experimental rate constant of 2.0×10^3 M^{-1} s^{-1}. Both experimental rate constants were determined from data obtained over the pH range of 4.0 to 10.0, where the diprotonated and monoprotonated Fe^{VI} are more involved than the non-protonated Fe^{VI}. As further validation, the ratio of the diprotonated/monoprotonated calculated rate constants is 14.3 compared to the experimental ratio of 13.5.

Six-Membered *R* versus Five-Membered *R* Containing SAs. Experimental results and theoretical calculations further support our proposed SO_2 mechanism for the oxidation of SDZ by Fe^{VI}, already corroborated by the energy computations for transition states, in that the formation of the five-membered ring transition state TS2, albeit a fleeting transient state, is indeed essential for SO_2 extrusion. It is interesting to note that SO_2 extrusion was not observed in SMX and other five-membered ring SAs (see Figures 1 and 2b). Identified OPs showed no extrusion step of the oxidation of SMX by Fe^{VI}, and reaction pathways have been described effectively by DFT calculations.[27] In SMX, the five-membered ring of the isoxazole places its N further away geometrically from the aniline ring C holding the S, than a six-membered ring would place the N of the pyrimidine ring. The SO_2**N**−**C**═**N** angle in SMX is about 122.3°, whereas it is 117.2° in SDZ as measured in semiempirical computations (see Figure 5). This is mainly a geometric difference.

Furthermore, the N of the isoxazole in SMX, which is bonded to the O, may have less propensity to curl around forming the "transient five-membered ring TS2" shown in Figure 5. Our DFT results show that the N in the isoxazole of SMX has more electron density (−0.21 atomic charge) than the N in pyrimidine of SDZ (−0.19 charge), plus the overall electronic density of the isoxazole ring in SMX (−0.12 net charge) is richer than that of the pyrimidine of SDZ (+0.05 net charge). This is likely a reason why Fe^{VI} breaks down the isoxazole ring, as seen in our previous work.[24] It is therefore plausible that the rate of −NH−SO_2−*R* oxidation in SMX is faster than the SO_2 extrusion, hence not observed in SMX, but observed in SDZ.

Implications. Previous experimental and theoretical calculations supported no extrusion of SO_2 during the oxidation of SAs containing five-membered heterocyclic moieties (e.g., SMX) by Fe^{VI}. However, a study of oxidized products and DFT calculations presented herein on the oxidation of SA with a six-membered heterocyclic moiety (e.g., SDZ) by Fe^{VI} indicate that the step of extrusion of SO_2 is involved, forming Fe^{V} and a radical. The presented mechanism of SO_2 extrusion may be possible for structurally similar six-membered heterocyclic containing SAs.

The species-specific rate constants of the reactions of Fe^{VI} with SAs could describe the experimental second-order rate constants of the oxidation of SAs by Fe^{VI}. The values of k at pH 7.0 and 8.0 were used to learn the half-lives ($t_{1/2}$) of the elimination of SAs by Fe^{VI}. If the concentration of Fe^{VI} is in excess over SAs at a dose of $[K_2FeO_4]$ = 10 mg L^{-1}, as may be expected in practical application, then the $t_{1/2}$ values of the reactions would be short and in the range from 12.52 s (SPY) to 361.20 s (SMIZ) at pH 8.0 and 25.0 °C (Figure S11). Because the values of k are pH-dependent, the $t_{1/2}$ values for the removal of SAs by Fe^{VI} would also vary with the solution pH. At pH 7.0, the $t_{1/2}$ values would be much shorter, from 8.14 s (SPY) to 173.74 s (SDM) (Figure S11). Variation in the dose of Fe^{VI} would also change the $t_{1/2}$ to remove SAs by Fe^{VI}.

■ ASSOCIATED CONTENT

Supporting Information

The Supporting Information is available free of charge on the ACS Publications website at DOI: 10.1021/acs.est.8b06535.

Texts S1−S3, information on chemicals, experimental procedures, and DFT calculations; Tables S1−S4, structural parameters of SAs and their correlation analysis with rate constants; Table 5, analysis data of SDZ, SIZ, and their OPs; Figure S1, self-decay of Fe^{VI} at different pH; Figures S2−S5, DFT calculations; Figure S6, the rate constants of reactions between Fe^{VI} and SAs at different pH; Figures S7 and S8, mass spectra of OPs; Figures S9 and S10, the reaction mechanisms; and Figure S11, the half-lives of the degradation of SAs by Fe^{VI} (PDF)

■ AUTHOR INFORMATION

Corresponding Authors

*E-mail: ching-hua.huang@ce.gatech.edu (C.-H.H.).
*E-mail: vsharma@sph.tamhsc.edu (V.K.S.).

ORCID

J. Clayton Baum: 0000-0003-0331-9730
Nasri Nesnas: 0000-0003-3511-940X
Yunho Lee: 0000-0001-5923-4897
Ching-Hua Huang: 0000-0002-3786-094X
Virender K. Sharma: 0000-0002-5980-8675

Notes

The authors declare no competing financial interest.

DOI: 10.1021/acs.est.8b06535
Environ. Sci. Technol. 2019, 53, 2695−2704

■ ACKNOWLEDGMENTS

V.K.S. acknowledges the financial support of the National Science Foundation (CBET 1802800). C.-H.H. thanks the NSF grants (CBET 1802944). We thank anonymous reviewers for their comments, which improved the paper.

■ REFERENCES

(1) Garner, E.; Chen, C.; Xia, K.; Bowers, J.; Engelthaler, D. M.; McLain, J.; Edwards, M. A.; Pruden, A. Metagenomic characterization of antibiotic resistance genes in full-scale reclaimed water distribution systems and corresponding potable systems. *Environ. Sci. Technol.* **2018**, *52* (11), 6113−6125.

(2) Jaffrézic, A.; Jardé, E.; Soulier, A.; Carrera, L.; Marengue, E.; Cailleau, A.; Le Bot, B. Veterinary pharmaceutical contamination in mixed land use watersheds: from agricultural headwater to water monitoring watershed. *Sci. Total Environ.* **2017**, *609*, 992−1000.

(3) Zhang, Q.; Ying, G.; Pan, C.; Liu, Y.; Zhao, J. Comprehensive evaluation of antibiotics emission and fate in the river basins of China: Source analysis, multimedia modeling, and linkage to bacterial resistance. *Environ. Sci. Technol.* **2015**, *49* (11), 6772−6782.

(4) aus der Beek, T.; Weber, F. A.; Bergmann, A.; Hickmann, S.; Ebert, I.; Hein, A.; Küster, A. Pharmaceuticals in the environment-Global occurrences and perspectives. *Environ. Toxicol. Chem.* **2016**, *35* (4), 823−835.

(5) Cizmas, L.; Sharma, V. K.; Gray, C.; McDonald, T. J. Pharmaceuticals and personal care products in waters: Occurrence, toxicity, and risk. *Environ. Chem. Lett.* **2015**, *13* (4), 381−394.

(6) Sharma, V. K.; Johnson, N.; Cizmas, L.; McDonald, T. J.; Kim, H. A review of the influence of treatment strategies on antibiotic resistant bacteria and antibiotic resistance genes. *Chemosphere* **2016**, *150*, 702−714.

(7) De Liguoro, M.; Riga, A.; Fariselli, P. Synergistic toxicity of some sulfonamide mixtures on Daphnia magna. *Ecotoxicol. Environ. Saf.* **2018**, *164*, 84−91.

(8) Wang, H.; Wang, N.; Wang, B.; Zhao, Q.; Fang, H.; Fu, C.; Tang, C.; Jiang, F.; Zhou, Y.; Chen, Y.; Jiang, Q. Antibiotics in drinking water in Shanghai and their contribution to antibiotic exposure of school children. *Environ. Sci. Technol.* **2016**, *50* (5), 2692−2699.

(9) Yang, H.; Zhuang, S.; Hu, Q.; Hu, L.; Yang, L.; Au, C.; Yi, B. Competitive reactions of hydroxyl and sulfate radicals with sulfonamides in $Fe^{2+}/S_2O_8^{2-}$ system: Reaction kinetics, degradation mechanism and acute toxicity. *Chem. Eng. J.* **2018**, *339*, 32−41.

(10) Yang, L.; Shi, Y.; Li, J.; Fang, L.; Luan, T. Transformation of aqueous sulfonamides under horseradish peroxidase and characterization of sulfur dioxide extrusion products from sulfadiazine. *Chemosphere* **2018**, *200*, 164−172.

(11) Nidheesh, P. V.; Olvera-Vargas, H.; Oturan, N.; Oturan, M. A. Heterogeneous electro-Fenton process: Principles and applications. *Handb. Environ. Chem.* **2017**, *61*, 85−110.

(12) Lee, Y.; von Gunten, U. Quantitative structure-activity relationships (QSARs) for the transformation of organic micropollutants during oxidative water treatment. *Water Res.* **2012**, *46* (19), 6177−6195.

(13) Wang, J.; Zhuan, R.; Chu, L. The occurrence, distribution and degradation of antibiotics by ionizing radiation: An overview. *Sci. Total Environ.* **2019**, *646*, 1385−1397.

(14) Chen, J.; Xie, S. Overview of sulfonamide biodegradation and the relevant pathways and microorganisms. *Sci. Total Environ.* **2018**, *640−641*, 1465−1477.

(15) Kim, H.; Hwang, Y. S.; Sharma, V. K. Adsorption of antibiotics and iopromide onto single-walled and multi-walled carbon nanotubes. *Chem. Eng. J.* **2014**, *255*, 23−27.

(16) Baena-Nogueras, R. M.; González-Mazo, E.; Lara-Martín, P. A. Photolysis of antibiotics under simulated sunlight irradiation: Identification of photoproducts by high-resolution mass spectrometry. *Environ. Sci. Technol.* **2017**, *51* (6), 3148−3156.

(17) Barhoumi, N.; Oturan, N.; Olvera-Vargas, H.; Brillas, E.; Gadri, A.; Ammar, S.; Oturan, M. A. Pyrite as a sustainable catalyst in electro-Fenton process for improving oxidation of sulfamethazine. Kinetics, mechanism and toxicity assessment. *Water Res.* **2016**, *94*, 52−61.

(18) Feng, Y.; Liao, C.; Kong, L.; Wu, D.; Liu, Y.; Lee, P.; Shih, K. Facile synthesis of highly reactive and stable Fe-doped g-C3N4composites for peroxymonosulfate activation: A novel non-radical oxidation process. *J. Hazard. Mater.* **2018**, *354*, 63−71.

(19) Shin, J.; Lee, D.; Hwang, T.; Lee, Y. Oxidation kinetics of algal-derived taste and odor compounds during water treatment with ferrate(VI). *Chem. Eng. J.* **2018**, *334*, 1065−1073.

(20) Shin, J.; Von Gunten, U.; Reckhow, D. A.; Allard, S.; Lee, Y. Reactions of ferrate(VI) with iodide and hypoiodous acid: Kinetics, pathways, and implications for the fate of iodine during water treatment. *Environ. Sci. Technol.* **2018**, *52* (13), 7458−7467.

(21) Karlesa, A.; De Vera, G. A. D.; Dodd, M. C.; Park, J.; Espino, M. P. B.; Lee, Y. Ferrate(VI) oxidation of ß-lactam antibiotics: Reaction kinetics, antibacterial activity changes, and transformation products. *Environ. Sci. Technol.* **2014**, *48* (17), 10380−10389.

(22) Liu, Y.; Wang, L.; Huang, Z.; Wang, X.; Zhao, X.; Ren, Y.; Sun, S.; Xue, M.; Qi, J.; Ma, J. Oxidation of odor compound indole in aqueous solution with ferrate(VI): Kinetics, pathway, and the variation of assimilable organic carbon. *Chem. Eng. J.* **2018**, *331*, 31−38.

(23) Sharma, V. K.; Chen, L.; Zboril, R. Review on high valent Fe^{VI} (ferrate): A sustainable green oxidant in organc chemistry and transformation of pharmaceuticals. *ACS Sustainable Chem. Eng.* **2016**, *4*, 18−34.

(24) Sharma, V. K.; Mishra, S. K.; Nesnas, N. Oxidation of sulfonamide antimicrobials by ferrate(VI) [$Fe^{VI}O_4^{2-}$]. *Environ. Sci. Technol.* **2006**, *40*, 7222−7227.

(25) Lee, Y.; Zimmermann, S. G.; Kieu, A. T.; von Gunten, U. Ferrate (Fe(VI)) application for municipal wastewater treatment: A novel process for simultaneous micropollutant oxidation and phosphate removal. *Environ. Sci. Technol.* **2009**, *43*, 3831−3838.

(26) Yang, B.; Ying, G. G.; Zhao, J. L.; Liu, S.; Zhou, L. J.; Chen, F. Removal of selected endocrine disrupting chemicals (EDCs) and pharmaceuticals and personal care products (PPCPs) during ferrate(VI) treatment of secondary wastewater effluents. *Water Res.* **2012**, *46* (7), 2194−2204.

(27) Yu, H.; Chen, J.; Xie, H.; Ge, P.; Kong, Q.; Luo, Y. Ferrate(vi) initiated oxidative degradation mechanisms clarified by DFT calculations: a case for sulfamethoxazole. *Environ. Sci. Process Impacts* **2017**, *19* (3), 370−378.

(28) Kim, C.; Panditi, V. R.; Gardinali, P. R.; Varma, R. S.; Kim, H.; Sharma, V. K. Ferrate promoted oxidative cleavage of sulfonamides: kinetics and product formation under acidic conditions. *Chem. Eng. J.* **2015**, *279*, 307−316.

(29) Feng, M.; Jinadatha, C.; McDonald, T. J.; Sharma, V. K. Accelerated oxidation of organic contaminants by ferrate(VI): The overlooked role of reducing additives. *Environ. Sci. Technol.* **2018**, *52* (19), 11319−11327.

(30) Boreen, A. L.; Arnold, W. A.; McNeill, K. Triplet-sensitized photodegradation of sulfa drugs containing six-membered heterocyclic groups: Identification of an SO_2 extrusion photoproduct. *Environ. Sci. Technol.* **2005**, *39* (10), 3630−3638.

(31) Feng, Y.; Wu, D.; Deng, Y.; Zhang, T.; Shih, K. Sulfate radical-mediated degradation of sulfadiazine by $CuFeO_2$ rhombohedral crystal-catalyzed peroxymonosulfate: Synergistic effects and mechanisms. *Environ. Sci. Technol.* **2016**, *50* (6), 3119−3127.

(32) Ji, Y.; Shi, Y.; Wang, L.; Lu, J.; Ferronato, C.; Chovelon, J. Sulfate radical-based oxidation of antibiotics sulfamethazine, sulfapyridine, sulfadiazine, sulfadimethoxine, and sulfachloropyridazine: Formation of SO_2 extrusion products and effects of natural organic matter. *Sci. Total Environ.* **2017**, *593−594*, 704−712.

(33) Fu, W.; Li, B.; Yang, J.; Yi, H.; Chai, L.; Li, X. New insights into the chlorination of sulfonamide: Smiles-type rearrangement, desulfation, and product toxicity. *Chem. Eng. J.* **2018**, *331*, 785−793.

DOI: 10.1021/acs.est.8b06535
Environ. Sci. Technol. 2019, 53, 2695−2704

(34) Yang, J.; He, M.; Wu, T.; Hao, A.; Zhang, S.; Chen, Y.; Zhou, S.; Zhen, L.; Wang, R.; Yuan, Z.; Deng, L. Sulfadiazine oxidation by permanganate: Kinetics, mechanistic investigation and toxicity evaluation. *Chem. Eng. J.* **2018**, *349*, 56−65.
(35) Tentscher, P. R.; Eustis, S. N.; McNeill, K.; Arey, J. S. Aqueous oxidation of sulfonamide antibiotics: Aromatic nucleophilic substitution of an aniline radical cation. *Chem. - Eur. J.* **2013**, *19* (34), 11216−11223.
(36) Feng, M.; Wang, X.; Chen, J.; Qu, R.; Sui, Y.; Cizmas, L.; Wang, Z.; Sharma, V. K. Degradation of fluoroquinolone antibiotics by ferrate(VI): Effects of water constituents and oxidized products. *Water Res.* **2016**, *103*, 48−57.
(37) Frisch, M. J.; Trucks, G. W.; Schlegel, H. B.; Scuseria, G. E.; Robb, M. A.; Cheeseman, J. R.; Scalmani, G.; Barone, V.; Petersson, G. A.; Nakatsuji, H.; Li, X.; Caricato, M.; Marenich, A.; Bloino, J.; Janesko, B. G.; Gomperts, R.; Mennucci, B.; Hratchian, H. P.; Ortiz, J. V.; Izmaylov, A. F.; Sonnenberg, J. L.; Williams-Young, D.; Ding, F.; Lipparini, F.; Egidi, F.; Goings, J.; Peng, B.; Petrone, A.; Henderson, T.; Ranasinghe, D.; Zakrzewski, V. G.; Gao, J.; Rega, N.; Zheng, G.; Liang, W.; Hada, M.; Ehara, M.; Toyota, K.; Fukuda, R.; Hasegawa, J.; Ishida, M.; Nakajima, T.; Honda, Y.; Kitao, O.; Nakai, H.; Vreven, T.; Throssell, K.; Montgomery, Jr., J. A.; Peralta, J. E.; Ogliaro, F.; Bearpark, M.; Heyd, J. J.; Brothers, E.; Kudin, K. N.; Staroverov, V. N.; Keith, T.; Kobayashi, R.; Normand, J.; Raghavachari, K.; Rendell, A.; Burant, J. C.; Iyengar, S. S.; Tomasi, J.; Cossi, M.; Millam, J. M.; Klene, M.; Adamo, C.; Cammi, R.; Ochterski, J. W.; Martin, R. L.; Morokuma, K.; Farkas, O.; Foresman, J. B.; Fox, D. J. *Gaussian 09*, Revision A.02; Gaussian, Inc.: Wallingford, CT, 2009.
(38) Zhao, Y.; Truhlar, D. G. The M06 suite of density functionals for main group thermochemistry, thermochemical kinetics, noncovalent interactions, excited states, and transition elements: Two new functionals and systematic testing of four M06-class functionals and 12 other functionals. *Theor. Chem. Acc.* **2008**, *120* (1−3), 215−241.
(39) Hirshfeld, F. L. Bonded-atom fragments for describing molecular charge densities. *Theoret. Chim. Acta* **1977**, *44* (2), 129−138.
(40) Ritchie, J. P.; Bachrach, S. M. Some methods and applications of electron density distribution analysis. *J. Comput. Chem.* **1987**, *8* (4), 499−509.
(41) Ritchie, J. P. Electron Density Distribution Analysis for Nitromethane, Nitromethide, and Nitramide. *J. Am. Chem. Soc.* **1985**, *107* (7), 1829−1837.
(42) Engel, T.; Reid, P. *Physical Chemistry*, 3rd ed.; Pearson: New York, 2013.
(43) Sharma, V. K.; Zboril, R.; Varma, R. S. Ferrates: Greener oxidants with multimodal action in water treatment technologies. *Acc. Chem. Res.* **2015**, *48* (2), 182−191.
(44) Sharma, V. K.; Burnett, C. R.; Millero, F. J. Dissociation constants of monoprotic ferrate(VI) ions in NaCl media. *Phys. Chem. Chem. Phys.* **2001**, *3*, 2059−2062.
(45) Zhang, R.; Yang, Y.; Huang, C. H.; Zhao, L.; Sun, P. Kinetics and modeling of sulfonamide antibiotic degradation in wastewater and human urine by UV/H_2O_2 and UV/PDS. *Water Res.* **2016**, *103*, 283−292.
(46) Focks, A.; Klasmeier, J.; Matthies, M. Mechanistic link between uptake of sulfonamides and bacteriostatic effect: Model development and application to experimental data from two soil microorganisms. *Environ. Toxicol. Chem.* **2010**, *29* (7), 1445−1452.
(47) Dmitrienko, S. G.; Kochuk, E. V.; Tolmacheva, V. V.; Apyari, V. V.; Zolotov, Y. A. Comparison of adsorbents for the preconcentration of sulfanilamides from aqueous solutions prior to HPLC determination. *J. Anal. Chem.* **2013**, *68* (10), 871−879.
(48) Anskjær, G. G.; Krogh, K. A.; Halling-Sørensen, B. Dialysis experiments for assessing the pH-dependent sorption of sulfonamides to soil clay fractions. *Chemosphere* **2014**, *95*, 116−123.
(49) Rush, J. D.; Bielski, B. H. J. Decay of ferrate(V) in neutral and acidic solutions. A premix pulse radiolysis study. *Inorg. Chem.* **1994**, *33*, 5499−5502.
(50) Terryn, R. J.; Huerta-Aguilar, C. A.; Baum, J. C.; Sharma, V. K. Fe^{VI}, Fe^{V}, and Fe^{IV} oxidation of cyanide: Elucidating the mechanism using density functional theory calculations. *Chem. Eng. J.* **2017**, *330*, 1272−1278.
(51) Kamachi, T.; Nakayama, T.; Yoshizawa, K. Mechanism and kinetics of cyanide decomposition by ferrate. *Bull. Chem. Soc. Jpn.* **2008**, *81*, 1212−1218.
(52) Ye, T.; Wei, Z.; Spinney, R.; Dionysiou, D. D.; Luo, S.; Chai, L.; Yang, Z.; Xiao, R. Quantitative structure−activity relationship for the apparent rate constants of aromatic contaminants oxidized by ferrate(VI). *Chem. Eng. J.* **2017**, *317*, 258−266.
(53) Lee, M.; Zimmermann-Steffens, S. G.; Arey, J. S.; Fenner, K.; Von Gunten, U. Development of prediction models for the reactivity of organic compounds with ozone in aqueous solution by quantum chemical calculations: The role of delocalized and localized molecular orbitals. *Environ. Sci. Technol.* **2015**, *49* (16), 9925−9935.
(54) Yang, Z.; Luo, S.; Wei, Z.; Ye, T.; Spinney, R.; Chen, D.; Xiao, R. Rate constants of hydroxyl radical oxidation of polychlorinated biphenyls in the gas phase: A single-descriptor based QSAR and DFT study. *Environ. Pollut.* **2016**, *211*, 157−164.
(55) Xiao, R.; Ye, T.; Wei, Z.; Luo, S.; Yang, Z.; Spinney, R. Quantitative Structure-Activity Relationship (QSAR) for the Oxidation of Trace Organic Contaminants by Sulfate Radical. *Environ. Sci. Technol.* **2015**, *49* (22), 13394−13402.
(56) Xu, X.; Xiao, R.; Dionysiou, D. D.; Spinney, R.; Fu, T.; Li, Q.; Wang, Z.; Wang, D.; Wei, Z. Kinetics and mechanisms of the formation of chlorinated and oxygenated polycyclic aromatic hydrocarbons during chlorination. *Chem. Eng. J.* **2018**, *351*, 248−257.
(57) Feng, M.; Cizmas, L.; Wang, Z.; Sharma, V. K. Synergistic effect of aqueous removal of fluoroquinolones by a combined use of peroxymonosulfate and ferrate(VI). *Chemosphere* **2017**, *177*, 144−148.
(58) Feng, M.; Qu, R.; Zhang, X.; Sun, P.; Sui, Y.; Wang, L.; Wang, Z. Degradation of flumequine in aqueous solution by persulfate activated with common methods and polyhydroquinone-coated magnetite/multi-walled carbon nanotubes catalysts. *Water Res.* **2015**, *85*, 1−10.
(59) Bielski, B. H. J.; Sharma, V. K.; Czapski, G. Reactivity of ferrate(V) with carboxylic acids: A pre-mix pulse radiolysis study. *Radiat. Phys. Chem.* **1994**, *44* (5), 479−484.
(60) Sharma, V. K. Ferrate(V) oxidation of pollutants: A premix pulse radiolysis. *Radiat. Phys. Chem.* **2002**, *65*, 349−355.

DOI: 10.1021/acs.est.8b06535
Environ. Sci. Technol. 2019, 53, 2695−2704